Design and mechanical analysis of additively manufactured primitive flexures

Jonah Leinwand[1], Mihaela Vlasea[1], Stewart McLachlin[1,*]

[1] Department of Mechanical and Mechatronics Engineering, University of Waterloo, Waterloo, Ontario, N2L 3G1, Canada

* stewart.mclachlin@uwaterloo.ca

Abstract: In the design of compliant mechanisms, thin flexural members, consisting of bends and curves, can be used to produce a controlled path of rotation under load, which could benefit the design of cervical artificial disc replacements (c-ADR) for example to improve compliance and avoid adjacent segment degeneration. However, to date, there is little literature to characterize the design and mechanical properties of additively manufactured flexural members, limiting crucial data needed to inform implant design. To address this knowledge gap, the goal of this work is to design and additively manufacture a family of primitive flexures to explore how different design features affect the resulting mechanical response under load. Several flexure primitive design features were varied within a common 3-prong flexure component design, including flexure thickness, overhang angle, and number of bends. The response of these designs was then analyzed through applied loading (non-destructive cyclic bending and compression to failure) based on a targeted application of a compliant mechanism for cervical artificial disc replacements. The ability to realize complex parts with latticed or flexible features has value in improving compliance in orthopaedic applications. The primitive flexure designs were printed using Ti6Al4V on the EOS M290 laser powder bed fusion system. For mechanical testing, the flexures were printed between custom-designed endplates to attach to the AMTI VIVO joint motion simulator. The deformation response was captured using the ARAMIS 3D digital image correlation system. Testing results indicated that thicknesses of at least 1mm were required in Ti6Al4V flexures to replicate the axial compressive stiffness in the cervical spine. Introduction of compliant flexure zones led to a negligible reduction in stiffness, while increasing structure compliance in compression and rotation.

Keywords: Laser Powder Bed Fusion, Compliant Mechanisms, Primitive Flexures, Mechanical Analysis.

1. Introduction

Compliant mechanisms are mechanical structures that achieve controlled deformation along a path through the elastic deformation of its members rather than the articulation of joints. Many types of compliant mechanisms currently exist, such as springs, or bending points of different thicknesses along a rigid body, as compiled by Howell [1, 2]. These mechanisms can be developed through different methodologies [1], but the critical aspect is the controlled deformation path [3]. Due to the complex geometries required for compliant mechanisms, additive manufacturing holds promise, with its compatibility in printing monolithic bodies and providing a lower time cost from design to product. Additive manufacturing has also become increasingly common in the orthopaedics space, being used to print complex geometries, porous materials, latticed structures, and osseo-integrative implant components [4-7].

Howell's method for design of compliant mechanisms [1, 2] involves creating a design library and then evaluating against design parameters for the design space. General considerations for compliant mechanisms include fatigue life of the design, material selection, stiffness, range of motion. For a target application of a cervical artificial disc replacement (c-ADR), it is important to also consider the biomechanics of the design space. Intervertebral discs (IVDs) are the primary joints between vertebrae, and are present in the cervical, thoracic, and lumbar spine. IVD biomechanics are complex, due to the anatomical differences in biological cell types in its' inner and outer sections. IVDs are made up of a soft squishy gel-like nucleus pulposus (NP) surrounded by a tough supportive annulus fibrosus (AF). IVDs carry the bulk of the compressive load in the cervical vertebral motion segment and experience flexion-extension, lateral bending, and axial torsion in the neck [8]. The IVD's stiffness in compression is reported as 800 N/mm [9]. While latticing has been used for implants such as spinal cages [10], latticing largely benefits bone growth and stability of the implant, whereas c-ADR requires highly controlled mobility under load, a task which flexures are better suited to through localized movement through elastic deformation. The introduction of flexures is aimed at addressing the gap of adjacent segment degeneration (ASD), which still occurs in 15-20% of c-ADR procedures [11].

In this study, we aim to design and additively manufacture a family of primitive flexures to explore how different design features affect the resulting mechanical response under load. It was hypothesized that, by developing better understanding of primitive features like flexure thickness, overhang angle, and number of bends, the flexural deformation response under bending and compressive loading could be optimized in future c-ADR designs to match the IVD behaviour.

2. Materials and Methods

2.1. Design Generation

The design space considered was with a 15x15mm rectangular footprint, and a height of 6mm, matching sizing data for current c-ADR [12]. The starting design space considered two 'endplates' to serve as hypothetical interfaces with superior and inferior vertebral endplates, with flexural elements connecting the endplates and providing the 'compliance profile' of the mechanism. Previous work on this topic by the same authors [13] showed that 2-element designs showed lower stiffness and weaker compressive strength than 3-element designs, so 3-element designs, such as the one shown in Figure 1, were the focus of this work, in an attempt to better match the target properties of c-ADR.

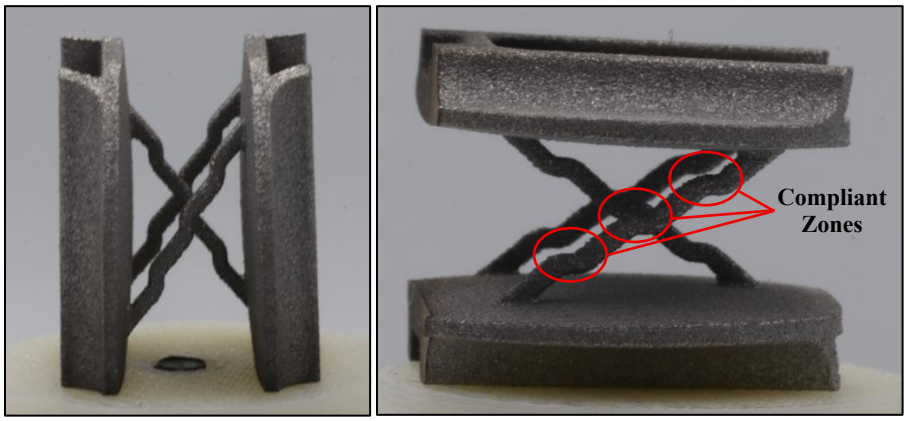

Figure 1. A sample flexure in the design space. Three flexure prongs with built-in compliant zones to allow for translation and rotation under loading, shown in the print orientation on the PBF-LB build plate (a-left) and its orientation under load (b-right)

The family of flexure elements considered have various properties that define their mechanical behaviour, such as thickness, overhang angle from the endplates, number of designed compliance zones, shape of the cross-sectional area, and infill variation, such as solid, hollow or latticed. The first three properties were selected for this work to observe the effect that variations had on the mechanical behaviour. In total, 10 different designs were generated, shown below in Table 1. Flexure types 1-7 all had 3 compliant zones per flexure, while Types 8-10 had 0, 1, and 2 compliant zones each respectively. These designs were all printed (n=3) via PBF-LB (EOS M290, EOS, Germany) in Ti6Al4V (AP&C – Ti-6Al-4V Grade 5, Grade 23 (Fine), AP&C, Canada).

Table 1. Code index with thicknesses and overhangs of printed parts. Types 1-4 were tested to study thickness, types 2, 5-7 to study overhang, and types 2, 8-10 to look at number of compliant zones per flexure

Type	Thickness [mm]	Overhang [deg]	Type	Thickness [mm]	Overhang [deg]
1	0.5	40	**6**	0.7	45
2	0.7	40	**7**	0.7	50
3	1	40	**8**	0.7	33.8
4	1.5	40	**9**	0.7	40
5	0.7	37.5	**10**	0.7	40

2.2. Design Evaluation

To characterize the mechanical behaviour using digital image correlation (DIC), each successfully manufactured flexure part was first painted with a white matte coat and then speckled with black spray paint, to produce a random distribution of points. Each flexure part was tested on the VIVO joint motion simulator (AMTI, USA) with a custom input waveform to provide three cycles at 0.05Hz of ±6° rotation in the plane of flexure rotation, about the axis perpendicular to the view shown in Figure 1b, followed by a compressive load from 0 to -1.8mm of displacement in the z-axis, at a rate of 0.1 strain/minute, per ISO 13314:2011. The Aramis 3D DIC system (Zeiss, Germany) was used to track the 3D displacement of the flexure members during the waveform. Data was recorded at a rate of 1Hz during the mechanical testing.

3. Results and discussion

All samples printed successfully, except for one type 1 part which broke upon receiving for analysis. All samples were able to successfully complete three cycles of ±6° rotation in the plane of flexure rotation. Porosity of a sample flexure was 0.02%, while average surface roughness measured on side-skin of a 1mm thickness flexure sample was 24.35um.

Flexure types 2-5, 8-10 had n=3 samples tested, while flexure types 6 and 7 had n=2 samples tested due to a mechanical equipment fault causing premature specimen failures. Axial stiffness values were calculated from the slopes of the force-displacement curves during compressive loading up to 30% strain, along with the measured axial load and measured axial strain of the flexures relative to the bottom endplate. Loads and axial displacements were reported at failure, or at the max value of 30% applied compressive strain. The average in-plane displacement of the flexures is reported during the ±6° of rotation, at the maximum range of motion of the flexures. The effect of thickness on these properties is shown in Table 2, from flexures of 0.5, 0.7, 1, and 1.5mm thickness (Types 1-4). The effect of overhang from the endplates is shown in Table 3, from flexures of 37.5, 40, 45, and 50 deg overhang (Types 5, 2, 6, 7). The effect of the number of compliant zones per flexure is shown in Table 4, from flexures with 0, 1, 2, and 3 compliant zones (Types 8-10, 2).

Table 2. Effect of flexure thickness on axial stiffness, compressive load and axial displacement at failure or test end (designated with *), and average in-plane flexure displacement during maximum range-of-motion

Type	Stiffness [N/mm]	Failure load [N]	Failure Z-disp [mm]	Avg. In-Plane disp. [mm]
1	815 ± 97	104.79 ± 16.27	0.13 ± 0.01	0.19 ± 0.00
2	3268 ± 1075	354.30 ± 14.56	0.12 ± 0.04	0.17 ± 0.00
3	11870 ± 1496	1027.70 ± 8.81*	0.09 ± 0.01*	0.16 ± 0.02
4	78861 ± 22378	1228.00 ± 6.10*	0.02 ± 0.00*	0.13 ± 0.01

Table 3. Effect of flexure overhang from the endplates on axial stiffness, compressive load and axial displacement at failure or test end, and average in-plane flexure displacement during maximum range-of-motion

Type	Stiffness [N/mm]	Failure load [N]	Failure Z-disp [mm]	Avg. In-Plane disp. [mm]
5	2536 ± 364	402.80 ± 1.30	0.16 ± 0.02	0.18 ± 0.01
2	3268 ± 1075	354.30 ± 14.60	0.12 ± 0.04	0.17 ± 0.00
6	1457 ± 58	263.00 ± 6.10	0.18 ± 0.00	0.18 ± 0.00
7	749 ± 318	207.10 ± 3.40	0.30 ± 0.12	0.19 ± 0.01

Table 4. Effect of number of compliant zones per flexure on axial stiffness, compressive load and axial displacement at failure or test end, and average in-plane flexure displacement during maximum range-of-motion

Type	Stiffness [N/mm]	Failure load [N]	Failure Z-disp [mm]	Avg. In-Plane disp. [mm]
8	3456 ± 105	494.40 ± 10.39	0.14 ± 0.01	0.16 ± 0.01
9	2912 ± 1189	399.10 ± 5.70	0.15 ± 0.05	0.15 ± 0.01
10	1765 ± 198	345.80 ± 5.20	0.20 ± 0.02	0.16 ± 0.01
2	3268 ± 1075	354.30 ± 14.60	0.12 ± 0.04	0.17 ± 0.00

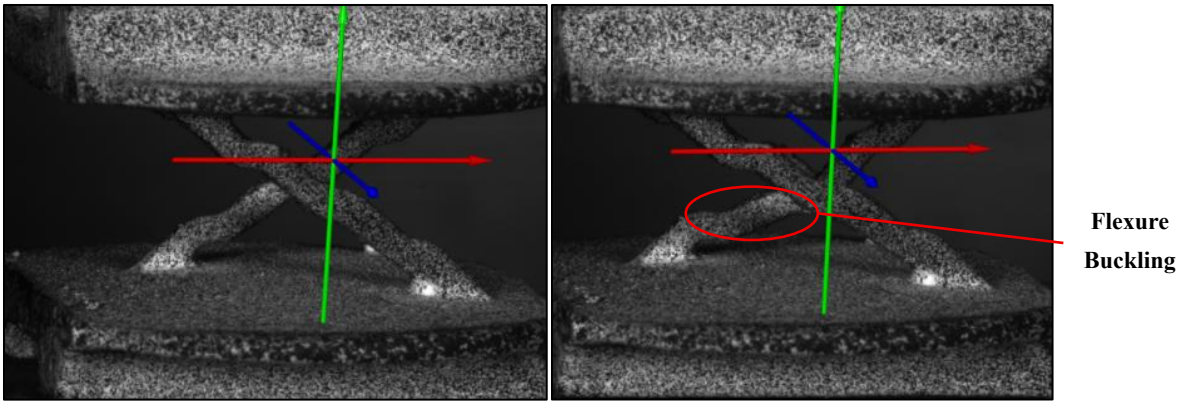

Figure 2. A measurement of a Type 2 sample flexure under axial compression at the start of the (left) and at the end (b-right). Flexures frequently failed due to buckling from the compressive force, in the middle of the flexure

There are several takeaways on the viability of different design features of a compliant flexure mechanism for a c-ADR implant design that can be taken from these results. Thicker flexures produced stiffer, stronger flexures that can withstand higher loads but experience smaller deformations, both in the axis of loading and in-plane during flexure rotation. Increasing the overhang angle of the flexures from their endplates both weakens and lowers the stiffness of the flexures in compressive loading. This is likely due to the greater ratio of 'horizontal components' present that reduces the amount

of material present to oppose the axial compressive force. Increasing the overhang angle increases the amount of displacement, both in the axis of loading and in-plane during rotation providing higher compliance. Increasing the number of compliant zones had insignificant effect on stiffness until a 3rd compliant zone was added, while it continually decreased the maximum compressive load of the flexures. It did increase the in-plane displacement during rotation, which suggests that the compliant zones succeed in making the flexure more compliant. Notably, introducing the first two compliant zones in the flexure path, had no effect on axial stiffness, while weaking failure load and increasing compliance during compression and rotation. This suggests adding a small number of compliant zones would be an effective method for increasing the compliance of thicker, stronger flexures in the desired plane of rotation.

There are limitations to this exploratory study for the design and analysis of primitive flexures. Due to the small number of samples printed for each flexure type, and with two flexure types having only two tested samples, no detailed statistical analysis was performed. However, the small variance in the mechanical analysis data does indicate reliable findings from additively manufactured primitive flexure design features that can be actioned in future c-ADR design concepts.

4. Conclusion

In the context of the targeted application of c-ADR, only flexure type 1 being 0.5mm thick achieved the same level of axial stiffness reported in literature for a c-ADR. A low to medium thickness flexure, 0.5-1mm in thickness, with an overhang angle ≥ 40deg from the endplates, and with multiple compliant zones would provide the appropriate mix of axial stiffness, axial strength, and rotational compliance to warrant further development as a c-ADR implant to help address ASD. Next steps include further characterization of flexure fatigue strength, both in compression and rotation, testing additional rotational moments to simulate the physiologic loading of axial torsion and lateral bending, as well as center of rotation effect from varying flexure parameters. This flexure testing is proposed before actualization of a flexure-based c-ADR implant, which would then require detailed investigation of the biocompatibility and surface characterization before clinical use.

5. Acknowledgments

Jonah Leinwand was supported by the Natural Sciences and Engineering Research Council of Canada Master's scholarship. This work was funded in part from the National Research Council of Canada, grant # A-0050173.

6. Conflicts of interest

The authors declare that they have no known competing financial interests or personal relationships that could have appeared to influence the work reported in these proceedings.

7. References

[1] Howell LL, Magleby SP, Olsen BM. Handbook of compliant mechanisms. John Wiley & Sons Ltd, Hoboken. 2013.
[2] Berglund MD, Magleby SP, Howell LL. Design rules for selecting and designing compliant mechanisms for rigid-body replacement synthesis. InInternational Design Engineering Technical Conferences and Computers and Information in Engineering Conference 2000 Sep 10 (Vol. 35128, pp. 233-241). American Society of Mechanical Engineers.
[3] Midha A, Norton TW, Howell LL. On the nomenclature, classification, and abstractions of compliant mechanisms.
[4] Bai L, Gong C, Chen X, Sun Y, Zhang J, Cai L, Zhu S, Xie SQ. Additive manufacturing of customized metallic orthopedic implants: Materials, structures, and surface modifications. Metals. 2019 Sep 12;9(9):1004.
[5] Abdudeen A, Abu Qudeiri JE, Kareem A, Valappil AK. Latest developments and insights of orthopedic implants in biomaterials using additive manufacturing technologies. Journal of Manufacturing and Materials Processing. 2022 Dec 14;6(6):162.
[6] Wang X, Xu S, Zhou S, Xu W, Leary M, Choong P, Qian M, Brandt M, Xie YM. Topological design and additive manufacturing of porous metals for bone scaffolds and orthopaedic implants: A review. Biomaterials. 2016 Mar 1;83:127-41.
[7] Germaini MM, Belhabib S, Guessasma S, Deterre R, Corre P, Weiss P. Additive manufacturing of biomaterials for bone tissue engineering–A critical review of the state of the art and new concepts. Progress in Materials Science. 2022 Oct 1;130:100963.
[8] Newell N, Little JP, Christou A, Adams MA, Adam CJ, Masouros SD. Biomechanics of the human intervertebral disc: a review of testing techniques and results. Journal of the mechanical behavior of biomedical materials. 2017 May 1;69:420-34.
[9] Shea M, Edwards WT, White AA, Hayes WC. Variations of stiffness and strength along the human cervical spine. Journal of biomechanics. 1991 Jan 1;24(2):95-107.
[10] Fogel G, Martin N, Lynch K, Pelletier MH, Wills D, Wang T, Walsh WR, Williams GM, Malik J, Peng Y, Jekir M. Subsidence and fusion performance of a 3D-printed porous interbody cage with stress-optimized body lattice and microporous endplates-a comprehensive mechanical and biological analysis. The Spine Journal. 2022 Jun 1;22(6):1028-37.
[11] Toci GR, Canseco JA, Patel PD, Divi SN, Goz V, Shenoy K, Sherman MB, Hilibrand AS, Donnally III CJ. The incidence of adjacent segment pathology after cervical disc arthroplasty compared with anterior cervical discectomy and fusion: a systematic review and meta-analysis of randomized clinical trials. World neurosurgery. 2022 Apr 1;160:e537-48.
[12] Shin JJ, Kim KR, Son DW, Shin DA, Yi S, Kim KN, Yoon DH, Ha Y, Riew KD. Cervical disc arthroplasty: what we know in 2020 and a literature review. Journal of Orthopaedic Surgery. 2021 Sep;29(1_suppl):23094990211006934.
[13] Leinwand J, McLachlin SD, A Novel Compliant Support Mechanism for Cervical Artificial Disc Replacement. Ontario Biomechanics Conference; 2023; Waterloo, ON, Canada.